

# More on the operator space entanglement ( $OSE$ ): Rényi $OSE$ , revivals, and integrability breaking.

Vincenzo Alba

<sup>1</sup>Dipartimento di Fisica dell'Università di Pisa and INFN, Sezione di Pisa, I-56127 Pisa, Italy

## Abstract.

We investigate the dynamics of the Rényi Operator Space Entanglement ( $OSE$ ) entropies  $S_n$  across several one-dimensional integrable and chaotic models. As a paradigmatic integrable system, we first consider the so-called rule 54 chain. Our numerical results reveal that the Rényi  $OSE$  entropies of diagonal operators with nonzero trace saturate at long times, in contrast with the behavior of von Neumann entropy. Oppositely, the Rényi entropies of traceless operators exhibit logarithmic growth with time, with the prefactor of this growth depending in a nontrivial manner on  $n$ . Notably, at long times, the complete operator entanglement spectrum ( $ES$ ) of an operator can be reconstructed from the spectrum of its traceless part. We observe a similar pattern in the  $XXZ$  chain, suggesting universal behavior. Additionally, we consider dynamics in nonintegrable deformations of the  $XXZ$  chain. Finite-time corrections do not allow to access the long-time behavior of the von Neumann entropy. On the other hand, for  $n > 1$  the growth of the entropies is milder, and it is compatible with a sublinear growth, at least for operators associated with global conserved quantities. Finally, we show that in finite-size integrable systems,  $S_n$  exhibit strong revivals, which are washed out when integrability is broken.

*This paper is dedicated to the memory of Marko Medenjak who left us before his time. In his brief journey Marko has left many important contributions that helped shape my interest in operator spreading. Our discussions stimulated many interesting questions, some of which are explored in this work.*

## 1. Introduction

The entanglement growth in typical out-of-equilibrium dynamics [1, 2, 3, 4, 5, 6] significantly hinders the simulation of out-of-equilibrium quantum many-body systems with state-of-the-art numerical methods, such as the time-dependent Density Matrix Renormalization Group [7, 8] (*tDMRG*). Early research into *tDMRG* suggested that instead of simulating the dynamics of the full quantum state, it could be convenient to focus on the Heisenberg dynamics of operators. The Heisenberg evolution of an operator  $\hat{\mathcal{O}}$  is expressed as

$$\hat{\mathcal{O}}(t) = \hat{U}^\dagger(t)\hat{\mathcal{O}}(0)\hat{U}(t), \quad \hat{U}(t) := e^{-iHt/\hbar}, \quad (1)$$

with  $H$  the Hamiltonian of the system. Here we restrict ourselves to one-dimensional lattice models (spin chains), considering a generic local operator  $\hat{\mathcal{O}}$  that acts nontrivially only at the center of the chain, and is the identity elsewhere (see Fig. 1). It is important to quantify the complexity of the operator growth, particularly by constructing the time-dependent Matrix Product Operator [8] (*MPO*) of  $\hat{\mathcal{O}}$ . Understanding the scaling of the bond dimension  $\chi$  of the *MPO* as a function of time is crucial. Initially, a double lightcone spreads from the center of the chain (see Fig. 1), as the operator support, i.e., the sites of the chain where the operator acts nontrivially, expands with time. This is typically accompanied by the growth of  $\chi$ . Based on exact results in noninteracting systems, Ref. [9] conjectured that there is a significant difference between integrable and nonintegrable dynamics: In integrable systems the bond dimension necessary for a fixed fidelity approximation of a local operator grows only polynomially with time, whereas nonintegrable Hamiltonians lead to an exponential growth of  $\chi$ .

The operator space entanglement (*OSE*) entropies [10]  $S_n(\hat{\mathcal{O}})$  provide a quantitative means to address these issues. To define  $S_n(\hat{\mathcal{O}})$  we bipartite the system as  $A \cup B$  (see Fig. 1), and consider the Schmidt decomposition of  $\hat{\mathcal{O}}(t)$  as

$$\frac{\hat{\mathcal{O}}(t)}{\sqrt{\text{Tr}(\hat{\mathcal{O}}^\dagger\hat{\mathcal{O}})}} = \sum_i \sqrt{\lambda_i} \hat{\mathcal{O}}_{A,i} \otimes \hat{\mathcal{O}}_{B,i}, \quad (2)$$

where  $\hat{\mathcal{O}}_{A/B,i}$  are two orthonormal sets of operators with support in  $A$  and  $B$ , satisfying  $\text{Tr}(\hat{\mathcal{O}}_{A/B,i}^\dagger \hat{\mathcal{O}}_{A/B,j}) = \delta_{ij}$ . In (17)  $\sqrt{\lambda_i} > 0$  are the so-called Schmidt coefficients. In the following we mostly consider the situation with  $A$  and  $B$  being two semi-infinite chains. We also fix  $x = 0$  (see Fig. 1), placing the boundary between  $A$  and  $B$  at the operator insertion. The Rényi *OSE* entropies  $S_n$  and the von Neumann one  $S_1$  are defined as

$$S_n(\hat{\mathcal{O}}) = \frac{1}{1-n} \ln \left( \sum_i \lambda_i^n \right), \quad S_1 = - \sum_i \lambda_i \ln(\lambda_i). \quad (3)$$

Now, according to the conjecture in Ref. [9], integrable dynamics lead to at most a logarithmic growth of  $S_n$  with time, whereas nonintegrable ones are expected to give linear growth of  $S_n$ . This scenario was first verified in noninteracting models [11, 12, 13]. Recently, it has been shown [14, 15] that the von Neumann *OSE* entropy can grow

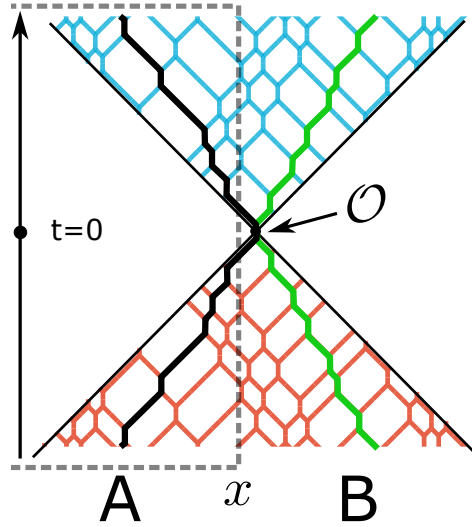


**Figure 1.** Setup considered in this work. We study the Heisenberg evolution  $\hat{\mathcal{O}}(t) = e^{iHt/\hbar}\hat{\mathcal{O}}e^{-iHt/\hbar}$  of a local operator  $\hat{\mathcal{O}}$  acting nontrivially at the center of a one dimensional system. Away from the center the operator acts as the identity. As time progresses, the support of the operator spreads, forming a double lightcone. For diagonal operators, the upper and lower parts of the lightcone coincide. We study the dynamics of the Rényi Operator Space Entanglement (*OSE*) entropies  $S_n(\hat{\mathcal{O}})$  ( $n \in \mathbb{N}$ ) of region A, starting at position  $x$ . Here we fix  $x = 0$ , meaning that A is the semi-infinite chain starting from the operator insertion. In the rule 54 chain the operator spreading is understood in terms of interacting left and right movers (solitons).

at most logarithmically with time in the rule 54 chain [16, 17], which has been studied intensively [18, 19, 20, 21, 22, 23] as a toy model of interacting integrable systems. Precisely, based on previous results in Ref. [24], Ref. [14] provided an algorithm to construct the *MPO* for a generic local operator  $\hat{\mathcal{O}}(t)$ . Crucially, the bond dimension  $\chi$  grows as  $t^2$ , which implies that  $S_n$  can grow only logarithmically with time. Moreover, Ref. [14] numerically showed that a similar logarithmic bound holds in Bethe ansatz solvable systems, such as the spin-1/2 Heisenberg *XXZ* chain. The linear-growth scenario for nonintegrable dynamics is supported by simulations in random unitary circuits, for which a so-called “membrane” picture for entanglement spreading applies [25, 26, 27, 28, 29]. Exact results in solvable chaotic quantum circuits [30, 31, 32, 33, 34, 35, 36] are also in agreement with the membrane picture.

Several open questions remain to be investigated. For instance, the underlying mechanism underlying the growth of the *OSE* has not been clarified yet. While Ref. [14] showed logarithmic growth for the *OSE* entropies in integrable systems, the prefactor of the logarithmic growth is not understood, except for some simple operators [15]. More importantly, the relationship between transport properties and operator spreading, if any, is yet to be unveiled. Still, it has been argued in Ref. [15] that the growth of the *OSE* of some simple operators reflects the diffusive fluctuations of the operator

front [37]. Furthermore, while a lot of attention has been devoted to the von Neumann *OSE* entropy, much less is known about the Rényi entropies, or the operator entanglement spectrum (*ES*) formed by the squared Schmidt values  $\{\lambda_i\}$  (cf. (2)). Clearly, it is of utmost importance to understand the scaling of *OSE* in nonintegrable Hamiltonians. Unfortunately, this is a daunting task from the numerical perspective, as *tDMRG* methods rely on the mild growth of the bond dimension with time. Interestingly, it has been suggested [38] (see also Section 3) that even in nonintegrable systems the *OSE* entropies of operators linked with global conservation laws could exhibit logarithmic growth with time, in contrast with the membrane-picture scenario.

Here we address some of these open questions focusing on diagonal operators. We first consider the dynamics of the Rényi entropies in the rule 54 chain. We show that there is a crucial distinction to be made between traceless operators and operators with nonzero trace. Precisely,  $S_n$  grow logarithmically for any  $n$  for traceless diagonal operators. The prefactor of the logarithmic growth depends on  $n$  in a nontrivial manner, and it is different from that governing the logarithmic growth of operators in noninteracting systems [13], which can be obtained with Conformal Field Theory (*CFT*) techniques. We also investigate the distribution of the operator entanglement spectrum levels, which shows marked differences with that obtained in Conformal Field Theories [39]. Oppositely, the entropies  $S_n$  of operators with nonzero trace grow logarithmically with time only for  $n = 1$ , in agreement with previous results [14, 15]. For  $n \neq 1$ ,  $S_n$  saturate at long times, the saturation values being fully determined by the trace of the operator. Interestingly, we show that the complete entanglement spectrum of an operator can be determined from the spectrum of its traceless part. We should mention that while the same results were presented as an approximation in Ref. [26], here we provide evidence that they become asymptotically exact in the long time limit. To address the universality of our results, we consider the spin-1/2 *XXZ* chain, which is a paradigmatic interacting integrable system. The same scenario uncovered for the rule 54 chain applies: Both the Rényi and the von Neumann entropies of traceless operators grow logarithmically with time for any  $n$ . Interestingly, within the accuracy of our *tDMRG* simulations, the dependence on  $n$  of the prefactors of the logarithmic growth is the same as in the rule 54 chain, suggesting the same underlying mechanism for operator spreading in the two models. The Rényi *OSE* entropies of operators with nonzero trace saturate at long time.

Next we consider the effects of breaking integrability, focusing on the *XXZ* chain with next-nearest-neighbor interactions. Although this deformed *XXZ* chain is not integrable, it commutes with the total magnetization. First, we observe that  $S_n$  exhibit strong finite-time corrections. This makes challenging to determine the asymptotic behavior of the von Neumann entropy at long times. On the other hand, our numerical results for  $S_n$  with  $n > 1$  are consistent with a quite mild growth in agreement with the bound of Ref. [38]. Finally, we investigate revival effects in finite-size chains. We show that for dynamics in the *XXZ* chain, which is integrable, the entropies exhibit revivals at times  $t \approx L/2$ . Revivals correspond to localized quasiparticles originated at

the center of the chain that re-enter subsystem  $A$  after bouncing back at the boundary of the system. Interestingly, in the presence of integrability-breaking interactions, the revivals are washed out, which reflects the absence of well-defined quasiparticles.

The manuscript is organized as follows. In Section 2 we introduce the rule 54 chain (in Section 2.1) and the deformed  $XXZ$  chain (in Section 2.1). In particular, in Section 2.1 we discuss some general results for operator spreading in integrable systems. In Section 3 we review exact results for the *OSE* entropies. Specifically, in Section 3.1 we focus on Ref. [38], which provided an exact bound between Rényi entropies and Out-of-Time-Order Correlators (*OTOC*). In Section 3.2, following Ref. [26], we discuss the relationship between the operator entanglement spectrum of traceless operators and that of operators with nonzero trace. In Section 3.3 we discuss the results of Ref. [15]. In Section 4 we present numerical *tDMRG* data for the dynamics of diagonal operators in the rule 54 chain. Precisely, in Section 4.1 we show that for operators with nonzero trace only the von Neumann entropy grows logarithmically, whereas the Rényi entropies saturate at long times. In Section 4.2 we show that the Rényi entropies of traceless operators grow logarithmically. The dynamics of the operator entanglement spectrum is discussed in Section 4.3. In Section 5 we focus on the  $XXZ$  chain. In Section 5.1 we compare the behavior of the Rényi entropies of traceless and operators with nonzero trace, showing that the same scenario discussed for the rule 54 chain in Section 4 applies. Section 5.2 is devoted to the effects of integrability breaking. In Section 5.3 we discuss revivals in finite-size integrable and nonintegrable systems. We conclude in Section 6.

## 2. Models & setup: Operator spreading in the rule 54 chain and the $XXZ$ chain

Here we introduce the two models that we will consider in this work, namely the so-called rule 54 chain and a nonintegrable deformation of the  $XXZ$  chain. Specifically, in Section 2.1 we discuss extensively the operator spreading in the rule 54 chain, as it is paradigmatic of generic integrable systems. In Section 2.2 we introduce the spin-1/2 Heisenberg  $XXZ$  chain with next-to-nearest-neighbor interactions, which allows to investigate both integrable and nonintegrable dynamics.

### 2.1. Rule 54 chain

The Hilbert space of the rule 54 chain [16] is that of a system of classical bits  $s_x = 0, 1$ . The system lives on a chain of  $L$  sites. The dynamics is generated by a three-site unitary gate  $U_x$  acting as

$$U_x = |s_{x-1}, s'_x, s_{x+1}\rangle\langle s_{x-1}s_x, s_{x+1}|, \quad (4)$$

where  $s'_x = s_{x-1} + s_{x+1} - s_{x-1}s_{x+1}$ . Precisely, one has

$$U_x = |101\rangle\langle 111| + |100\rangle\langle 110| + |111\rangle\langle 101| + |110\rangle\langle 100| \\ + |001\rangle\langle 011| + |010\rangle\langle 010| + |011\rangle\langle 001| + |000\rangle\langle 000|. \quad (5)$$

As it is clear from (4) and (5),  $U_x$  flips the bit at position  $x$  if at least one of its neighboring bits at  $x-1$  and  $x+1$  is in the state 1. Any bit configuration is evolved by applying  $U_x$  in a “brick-wall” fashion as  $U = \prod_{\text{even } x} \prod_{\text{odd } x} U_x$ . Time is discrete in units of 1. Clearly, Eq. (4) maps classical bit strings into classical bit strings. The rule 54 chain possesses well-defined quasiparticles (see Fig. 1), which is the key property of generic integrable systems. Quasiparticles are emergent left/right moving solitons. Precisely, solitons are formed by pairs of adjacent bits that are in the 1 state. Depending on the parity of the site of the leftmost 1 of the pair, they are left or right moving solitons [24]. The velocity of the solitons is  $v = \pm 1$ . Solitons are interacting, undergoing pairwise elastic scattering. The scattering is implemented as a Wigner time delay [40]. Precisely, when a left and a right moving soliton meet at the same site, they merge giving rise to the configuration  $\dots 010 \dots$ . The solitons remain “bound” together for a unit of time, before re-emerging as distinct left and right movers (several scattering processes are shown in Fig. 1). Again, this behavior is reminiscent of generic integrable models, which exhibit factorized two-body elastic scattering. The major difference is that in generic integrable models the quasiparticles possess a nontrivial dispersion, implying that their energies and velocities depend on a real parameter  $\lambda$ , which labels the different quasiparticles. It is important to stress that there is a mapping between the soliton basis and the standard bit basis. The mapping can be represented as an *MPO*. By applying the *MPO* on a generic string of bits, one obtains the corresponding configuration of left and right movers. Crucially, the mapping is local, because to determine whether at a generic site  $x$  there is a left or right moving soliton, only the bit configuration of the neighboring sites is needed. This implies that the mapping can be represented as an *MPO* with finite bond dimension  $\chi$  (see Ref. [14] and [15] for the explicit mapping). The bond dimension of the *MPO* that encodes the mapping does not depend on time, and cannot affect the leading behavior of the operator entanglement in the large time limit.

Let us now discuss operator spreading in the rule 54 chain. First, let us observe that the identity operator is

$$\mathbb{1} = \prod_x (|0\rangle\langle 0| + |1\rangle\langle 1|)_x, \quad (6)$$

where the subscript  $x$  means that the operator lives in the Hilbert space at site  $x$ . Upon expanding the product in (6), one obtains the equal-weight superposition of all the terms with an arbitrary number of projectors  $|0\rangle\langle 0|$  and  $|1\rangle\langle 1|$ . The identity commutes with the evolution operator, meaning that the equal-weight superposition is mapped onto itself under the dynamics. The *MPO* representing the identity has bond dimension  $\chi = 1$ . This is evident from the fact that in the bit basis, irrespective of the local projector present at site  $x$ , the neighboring sites at  $x+1$  and  $x-1$  can have both  $|0\rangle\langle 0|$  or  $|1\rangle\langle 1|$ . This implies that  $S_n(\mathbb{1}) = 0$  for any  $n$ , and at any time. In a similar way, after rewriting the evolution of the identity operator in terms of solitons, one obtains the equal-weight superposition of all the configurations with an arbitrary number of right and left movers.

One should observe that, since the mapping between bits and solitons has finite  $\chi > 1$ , one obtains that  $S_n(\mathbb{1}) = \mathcal{O}(1)$  for any time.

This changes dramatically if an operator  $\mathcal{O}$  is inserted at the center of the system, because the bond dimension of the *MPO* of the operator starts growing with time. Specifically, a double lightcone forms (see Fig. 1), as information propagates away from the operator insertion at finite velocity. The *MPO* of the operator has bond dimension  $\chi = 1$  outside of the lightcone, whereas inside its bond dimension grows. The reason is that the operator insertion puts nonlocal constraints on the motion of the left and right movers. To illustrate that, we now focus on the spreading of diagonal operators, for which the double-lightcone is symmetric, i.e., its upper part coincides with its lower one. Specifically we consider the local projector operator  $P_z$  acting at the center of the system, and  $S_{L/2}^z$ , defined as

$$P_z := \frac{1}{2} \left( \mathbb{1} + \sigma_{L/2}^z \right) = |1\rangle\langle 1|, \quad S_{L/2}^z := \sigma_{L/2}^z, \quad (7)$$

with  $\sigma_x^z$  the Pauli matrix acting at site  $L/2$ . Notice that while  $S^z$  is a traceless operator,  $P_z$  has a nonzero trace. Operator spreading is better understood in the soliton basis [14]. To represent  $P_z$  in the basis of left and right movers, it is convenient to expand  $\mathbb{1}_{L/2-1} P_z \mathbb{1}_{L/2+1}$  as

$$\mathbb{1}_{L/2-1} P_z \mathbb{1}_{L/2+1} = |010\rangle\langle 010| + |011\rangle\langle 011| + |110\rangle\langle 110| + |111\rangle\langle 111|. \quad (8)$$

The first term in (8) creates a pair of scattering solitons (as depicted in Fig. 1), whereas the second and third one creates a left and a right moving soliton at the center, respectively. Upon applying the evolution operator (4) the solitons created by the insertion of the operator propagate, scattering with the background solitons away from the center. This means that at a generic time  $t$  any allowed soliton configuration in the light cone has to contain the solitons that were created by the operator insertion at  $t = 0$ , although their positions are shifted by the scatterings with the background solitons (see Fig. 1). All the *allowed* soliton configurations at time  $t$  have the same amplitude. One can show that the bond dimension of the evolved *MPO* is determined by the number of steps to decide whether a generic soliton configuration in the lightcone is allowed or not [24, 14]. Equivalently, this is the number of steps needed to identify the positions at time  $t$  of the solitons that emerged from the center of the chain, and it grows as  $t^2$ . Importantly, the fact that  $\chi = \mathcal{O}(t^2)$  provides only a bound on the growth of the *OSE* entropies. Indeed, by assuming that all the  $\chi$  Schmidt values in (2) are the same, one obtains  $S_1 \propto 2 \ln(t)$ . On the other hand, Ref. [14] provided numerical evidence that  $S_1 \propto \ln(t)$  for the operator  $S^z$  and  $S_1 \propto 1/2 \ln(t)$  for  $P_z$  [15]. This means that the exact *MPOs* describing the dynamics of local operators contain too much information and can be further compressed. The reason why this is possible has not been clarified yet.

However, it has been argued in Ref. [15] that the growth of the *OSE* entropy reflects the diffusive quasiparticle spreading. Indeed, as a consequence of the interactions, the trajectory of the solitons (both the ones produced at the center and the background



ones) exhibits diffusion. If one imagine of coarse graining the dynamics, one has that the effect of interactions, at long times and large distances, is a renormalization of the soliton velocities [17]. In the coarse-grained picture, the solitons move with their renormalized velocities as free particles, i.e., without scattering. Now, the dynamics resembles that of the identity operator, implying that the operator entanglement does not grow. This suggests that the growth of the *OSE* could be attributed to the diffusive fluctuations of the solitons trajectories.

## 2.2. Spin-1/2 *XXZ* chain and its nonintegrable deformation

In this work we also consider a nonintegrable deformation of the spin-1/2 Heisenberg *XXZ* chain defined by the Hamiltonian

$$H = \sum_{x=1}^{L-1} \frac{1}{2} (S_x^+ S_{x+1}^- + S_x^- S_{x+1}^+) + \Delta \sum_{x=1}^{L-1} S_x^z S_{x+1}^z + \Delta' \sum_{x=1}^{L-2} S_x^z S_{x+2}^z. \quad (9)$$

Here  $S_x^\pm$  are standard raising/lowering spin-1/2 operators acting at site  $x$ , and  $\Delta, \Delta'$  are real parameters. For  $\Delta = \Delta' = 0$  the model (9) can be mapped to a system of noninteracting fermions. For  $\Delta' = 0$ , Eq. (9) becomes the *XXZ* chain, which is a prototypical Bethe ansatz solvable model [41]. For nonzero  $\Delta'$  the model is nonintegrable, as one can show by studying the statistics of the gaps in the energy spectrum [15]. As for the rule 54 chain, we focus on the spreading of the diagonal operators  $S^z$  and  $P_z$ , defined in (7). The *XXZ* chain possesses well-defined quasiparticles, which are at the heart of the quasiparticle picture [5, 42] for entanglement spreading and of Generalized Hydrodynamics [43, 44]. In contrast with the rule 54 chain, for which one can construct explicitly the *MPO* describing a generic time-dependent operator, it is much more challenging to obtain exact results for operator spreading in the *XXZ* chain (9), even in the integrable case for  $\Delta' = 0$ . However, it has been numerically shown in Ref. [14] that for  $\Delta' = 0$  the *OSE* entropy grows logarithmically with time for generic  $\Delta$ . In particular, Ref. [15] showed that for  $\Delta' = 0$ ,  $S_1(P_z)$  grows as  $1/2 \ln(t)$ , for any  $\Delta$ , which is the same behavior observed in the rule 54 chain. The dynamics of  $S_1(S^z)$  is compatible with a logarithmic growth as  $S_1(S^z) \approx \ln(t)$ . Finally, for  $\Delta' \neq 0$ , numerical results for the growth of the *OSE* are inconclusive due to strong finite-time effects [15].

## 3. Analytical bounds on the growth of the *OSE* entropies

Let us now discuss some analytical results that are available for the *OSE* entropies in generic systems. In Section 3.1 we review the result of Ref. [38], showing that the *OSE* entropies of a given operator  $\mathcal{O}$  can be bound by its Out-of-Time-Order Correlator (*OTOC*). In Section 3.2, following Ref. [26] we argue that the *OSE* of an operator is determined by its traceless part. Finally, in Section 3.3 we review the results of Ref. [15] trying to establish a relationship between the growth of *OSE* and diffusion.



### 3.1. Operator entanglement and OTOC: The bound of Ref. [38]

Ref. [38] showed that for  $n > 1$  the Rényi OSE entropies  $S_n(\hat{\mathcal{O}})$  of a generic local operator  $\hat{\mathcal{O}}$  is bound by its OTOC as

$$S_n(\hat{\mathcal{O}}) \leq \frac{2n}{1-n} \ln |\langle \hat{\mathcal{O}}^\dagger(t) \hat{\mathcal{O}}(0) \rangle_{T=\infty}|, \quad n > 1, \quad (10)$$

where  $\langle \hat{\mathcal{O}}_1 \hat{\mathcal{O}}_2 \rangle_{T=\infty} = \text{Tr}(\hat{\mathcal{O}}_1 \hat{\mathcal{O}}_2)$ . The derivation of (10) is straightforward, and we report it for completeness. One starts from the decomposition

$$\frac{\hat{\mathcal{O}}(t)}{\sqrt{\text{Tr}(\hat{\mathcal{O}}^\dagger \hat{\mathcal{O}})}} = \sum_{rs} \Lambda_{rs}(t) \hat{\mathcal{O}}_{r,A} \otimes \hat{\mathcal{O}}_{s,B}, \quad (11)$$

where  $\Lambda_{rs}$  is a time-dependent matrix, and  $\hat{\mathcal{O}}_{r,A}$  and  $\hat{\mathcal{O}}_{s,B}$  form two time-independent orthonormal bases for the operators with support in  $A$  and  $B$ , i.e., satisfying  $\text{Tr}(\hat{\mathcal{O}}_{r,A(B)}^\dagger \hat{\mathcal{O}}_{r',A(B)}) = \delta_{rr'}$ . One can perform a Singular Value Decomposition of  $\Lambda_{rs}$  to obtain

$$\frac{\hat{\mathcal{O}}(t)}{\sqrt{\text{Tr}(\hat{\mathcal{O}}^\dagger \hat{\mathcal{O}})}} = \sum_r \sqrt{\lambda_r(t)} \hat{\tilde{\mathcal{O}}}_{r,A}(t) \otimes \hat{\tilde{\mathcal{O}}}_{r,B}(t), \quad (12)$$

where  $\sqrt{\lambda_r}$  are the Schmidt values, and the operators appearing in the right-hand side of (12) depend on time and are orthonormal. We now obtain the chain of inequalities as [38]

$$\begin{aligned} |\langle \hat{\mathcal{O}}^\dagger(t) \hat{\mathcal{O}}(0) \rangle_{T=\infty}| &= |\text{Tr}(\Lambda^\dagger(t) \Lambda(0))| \leq \left| \sum_k \sqrt{\lambda_k(t) \lambda_k(0)} \right| \\ &\leq \kappa_0 \left( \sum_k \frac{\sqrt{\lambda_k(0)}}{\kappa_0} \lambda_k^{n/2} \right)^{1/n} \leq \kappa_0^{1-1/n} \left( \sum_k \lambda_k^n \right)^{1/(2n)}, \quad \kappa_0 := \sum_k \sqrt{\lambda_k(0)}. \end{aligned} \quad (13)$$

In the first row in (13) we used the von Neuman trace inequality [45]  $|\text{Tr}(XY)| \leq \sum_j \alpha_j \beta_j$ , with  $\alpha_j, \beta_j$  the singular values obtained from the Schmidt decomposition of  $X$  and  $Y$ , respectively. In the second row of (13) we first employed the Jensen inequality, and then the Cauchy-Schwartz inequality. For local product operators  $\kappa_0 = 1$ . By taking the logarithm of both members of (13) and multiplying them by  $2n/(1-n)$ , one obtains (10).

Let us now focus on the OTOC on the left-hand side of (10). One should expect a vanishing behavior in the limit  $t \rightarrow \infty$ , although several scenarios are possible. Ballistic spreading of operators, as in integrable systems, suggests power-law [46] decay as  $1/t$  in the limit  $t \rightarrow \infty$ , whereas diffusive spreading corresponds to the slower decay as  $1/\sqrt{t}$ . From (10), power-law decay of the OTOC implies a logarithmic growth of the OSE. On the other hand, for some operators the OTOC in (10) decays exponentially with time. For instance, this happens for the correlator  $\langle S^+(t) S^- \rangle$  in the  $XX$  spin chain [47]. In these situations, Eq. (10) gives a linear bound for the OSE entropies. However, the bound (10) is generically not saturated. For instance, it is well-know that in the  $XX$  chain the OSE entropy of  $S^+$  grows logarithmically with time [12, 11, 13].

Similarly, if Eq. (10) is saturated for  $S^z$ , one has a logarithmic growth of the *OSE*, as  $S_n(S^z) \sim 2n/(n-1) \ln(t)$  since  $\langle S^z(t)S^z(0) \rangle \sim 1/t$  at long times [47]. On the other hand, it is well-known that  $S_n(S^z)$  saturates to a constant at long times [12, 13]. We conclude that Eq. (10) is in general a loose bound on the *OSE* growth.

### 3.2. Traceless versus traceful operators (Ref. [26])

Following Ref. [26], one can argue that the dynamics of  $S_n(\hat{O})$  can be obtained from  $S_n(\hat{O}')$ , where  $\hat{O}'$  is the traceless part of  $\hat{O}$ . Let us decompose the generic normalized operator  $\hat{O}$  as

$$\hat{O} := \sqrt{p}\mathbb{1} + \sqrt{1-p}\hat{O}' \quad \sqrt{p} := \text{Tr}(\hat{O}), \quad (14)$$

where  $\hat{O}'$  is traceless and both  $\hat{O}'$  and  $\mathbb{1}$  are normalized. The time-evolved operator  $\hat{O}(t)$  can be decomposed as

$$\hat{O}(t) := \sqrt{p}\mathbb{1} + \sqrt{1-p}\hat{O}'(t), \quad (15)$$

and  $\hat{O}'(t)$  is traceless. After performing a Schmidt decomposition of  $\hat{O}'$ , we obtain

$$\hat{O}(t) = \sqrt{p}\mathbb{1}_A \otimes \mathbb{1}_B + \sum_i \sqrt{(1-p)\lambda'_i(t)} \hat{O}'_{A,i}(t) \otimes \hat{O}'_{B,i}(t), \quad (16)$$

where  $\lambda'_i(t) \geq 0$  are the Schmidt values. In general one should expect that at least some of the operators  $\hat{O}'_{A,i}$  appearing in the second term in (16) will develop a nonzero trace, i.e., they will not be orthogonal to the identity  $\mathbb{1}_A$ , implying that Eq. (16) is not a Schmidt decomposition for  $\hat{O}(t)$ . If we assume that all the  $\hat{O}'_{A,i}$  are traceless, then Eq. (16) is a Schmidt decomposition for  $\hat{O}(t)$ . This implies that the operator entanglement spectrum  $\{\lambda_i\}$  of  $\hat{O}(t)$  can be decomposed as

$$\{\lambda_j\} = \{p\} \cup \{(1-p)\lambda'_i\}, \quad (17)$$

where  $\lambda_i$  are the same as in (16). Eq. (18) implies that the *OSE* of a given operator  $\hat{O}$  can be determined by that of its traceless part  $\hat{O}'$ . Specifically, for the von Neumann entropy one has

$$S(\hat{O}) = p \ln(p) + (1-p) \sum_i \lambda'_i \ln(1-p) + (1-p)S(\hat{O}') = (1-p)S(\hat{O}'), \quad (18)$$

where in the last step we used that  $\sum_i \lambda'_i = 1$ .

Similarly, the Rényi entropy satisfy

$$S_n(\hat{O}) = \frac{1}{1-n} \ln \left[ p^n + (1-p) \sum_i \lambda_i'^n \right] \approx \frac{n}{1-n} \ln(p), \quad (19)$$

where we used that at long times  $\sum_i \lambda_i'^n \rightarrow 0$  because the operator support increases, while  $\sum_i \lambda_i' = 1$  because the operators are normalized. As we will discuss in Section 4 and Section 5, the decomposition (17) captures correctly the dynamics of the *OSE*, at least at long times and for large subsystems  $A$ . In particular, let us consider the case in which  $A$  is half of the system, as in Fig. 1. Now, at short times, when the light cone is “small” (see Fig. 1), it is likely that some of the  $\hat{O}'_{A,i}$  in the right-hand side in (16) contain the identity operator, whereas at long times the probability of generating the identity in the whole subsystem  $A$  is suppressed.

### 3.3. Operator space entanglement and diffusion (Ref. [15])

Inspired by the results for the rule 54 chain, a plausible scenario is that the dynamics of the operator entanglement reflects the diffusive dynamics of the underlying solitons [15], as discussed already in Section 2.1. Again, at a ballistic level, or at a coarse-grained level, the left and right movers behave as noninteracting particles, moving with effective velocities, which are determined by the scatterings. This also applies to the solitons produced at the center of the chain by the operator insertion. Since at a ballistic level the solitons behave as free particles, the operator entanglement does not grow [48]. Still, it is challenging to encapsulate this idea in a quantitative framework. As suggested in Ref. [15], a crude approximation for the Schmidt decomposition of an operator  $\hat{O}$  is

$$\hat{O}(t) = \sum_{k=0}^{t-|x|} \frac{\sqrt{\binom{t-|x|}{k} \binom{t+|x|}{t-k}}}{\sqrt{\binom{2t}{t}}} \hat{O}_{A,k} \otimes \hat{O}_{B,t-k}. \quad (20)$$

In (20),  $\hat{O}_{A,k}$  and  $\hat{O}_{B,t-k}$  are normalized operators in  $A$  and  $B$  constructed with  $k$  and  $t-k$  solitons. In (20) we assume that  $\hat{O}_{A,k}$  and  $\hat{O}_{B,t-k}$  are some “flat” superpositions of all the configurations with  $k$  and  $t-k$  solitons. Physically, this means that the scatterings maximally “scramble” the trajectories of the solitons within the lightcone. In (20),  $x$  is the position of the cut dividing subsystem  $A$  from  $B$  (see Fig. 1). The two binomials in (17) are the number of ways of arranging the solitons in  $A$  and  $B$ . In the limit  $t \rightarrow \infty$  the coefficients in (20) are dominated by the term with  $k = (t - |x|)/2$ , with diffusive fluctuations as  $\sqrt{t}$ . Now, the decomposition in (20) is an approximation because interactions are local and the trajectories of the solitons cannot be scattered at arbitrary distances. The bond dimension of the decomposition in (17) is  $t - |x| + 1$ . Notice that  $t - |x|$  is the largest number of solitons that can be accommodated within  $A$ . Notice also that Eq. (20) implies that there are only  $\propto t$  nonzero Schmidt values, whereas the exact *MPO* describing the dynamics of generic operators has  $\sim t^2$  nonzero Schmidt values [14]. By using (20), one obtains the analytical result for the von Neumann entropy as

$$S_n = \frac{1}{2} \ln(t), \quad \forall n. \quad (21)$$

Thus, Eq. (20) implies that the Rényi *OSE* entropies should not depend on  $n$ . The prefactor  $1/2$  of the logarithmic growth clearly reflects the diffusive spreading of the solitons trajectories. As it will be clear in the following, this is not the case, signaling that Eq. (20) does not capture correctly the detailed structure of the operator entanglement spectrum. On the other hand, Eq. (21) is in agreement with the growth of the von Neumann entropy of the projector operator  $P_z$  (see Ref. [15]).

## 4. Rényi entanglement of operators in the rule 54 chain: A *tDMRG* analysis

Here we discuss *tDMRG* results for  $S_n$  of diagonal operators in the rule 54 chain. In particular, in Section 4.1 we show that given an operator  $\hat{O}$  with nonzero trace,  $S_1(\hat{O})$

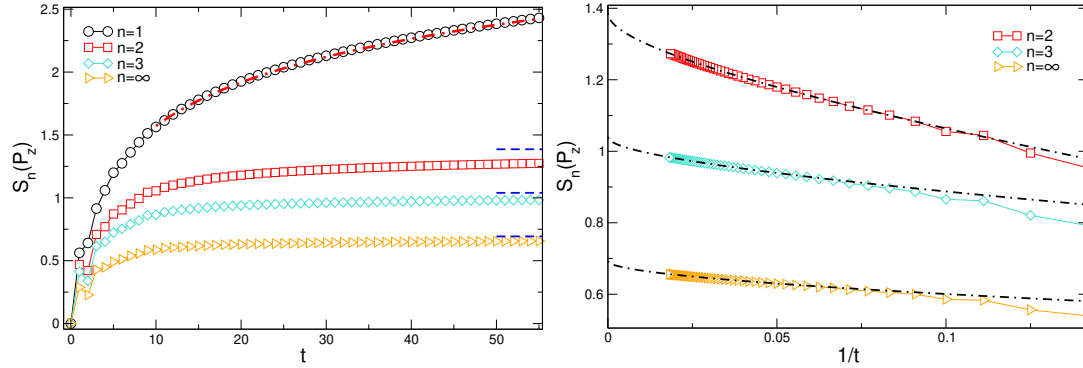


**Figure 2.** Dynamics of the Rényi operator entanglement entropies  $S_n$  for the projector operator  $P_z$  in the rule 54 chain. Left panel:  $tDMRG$  data for  $S_n$  plotted versus time  $t$  for several values of  $n$ . The dashed-dotted line is the behavior  $S_1 = a \ln(t) + b$ , with  $a, b$  a fitting parameter. The fit gives  $a = 0.50(1)$ . The horizontal lines are  $S_n = n/(n-1) \ln(p)$  (cf. Eq. (19)) with  $p = 1/2$ . Right panel: Same data as in the left panel plotting  $S_n - n/(n-1) \ln(2)$  versus  $1/t$  for  $n > 1$ . The dashed-dotted lines are fits to  $S_n = n/(n-1) \ln(2) + a_1/t^{1/2} + a_2/t$ , with  $a_1, a_2$  fitting parameters.

can be obtained from  $S_1(\hat{\mathcal{O}}')$ , with  $\hat{\mathcal{O}}'$  the traceless part of the operator. Moreover, we show that  $S_n$  saturate to a constant value in the limit  $t \rightarrow \infty$ , in agreement with the results of Section 3.2. In Section 4.2 we focus on traceless operators. We numerically show that  $S_n$  is compatible with a logarithmic growth for any  $n$ , although the prefactor of the logarithmic growth depends on  $n$  in a nontrivial manner. Finally, in Section 4.3 we discuss how this is reflected in the distribution of the levels of the operator entanglement spectrum.

#### 4.1. Dynamics of the Rényi entropies for $P_z$ : Effect of a nonzero trace

In Fig. 2 we show  $tDMRG$  data for  $S_n$  of the spin projector operator  $P_z$  (cf. (7)). Our  $tDMRG$  simulations are performed at fixed bond dimension  $\chi = 1600$ , which allows us to reach times  $t \approx 60$ . As it is clear from Fig. 2 (left panel),  $S_n(P_z)$  increase with time, although the dynamics is much slower for  $n > 1$ , as compared with  $n = 1$ . The growth of  $S_1(P_z)$  was investigated in Ref. [14] and Ref. [15], and it is compatible with the behavior  $S_1(P_z) \sim 1/2 \ln(t)$ , i.e., Eq. (21). The dashed-dotted line in the left panel of Fig. 2 is

$$S_n = a \ln(t) + b, \quad (22)$$

with  $a, b$  fitting parameters. To obtain  $a, b$  we fitted the data in the range  $t_{min} \leq t \leq 50$  to (22), i.e., discarding the short times with  $t \leq t_{min}$  because Eq. (22) is valid only at asymptotically long times. We estimated the error on  $a$  by monitoring its variation when increasing  $t_{min}$ . We should observe that by fitting the data for  $n > 1$  to (22) we obtain quite “small” values for  $a$  as  $a \approx 0.08, 0.04, 0.02$  for  $n, 2, 3, \infty$ . However, as we now discuss, this signals that Eq. (22) does not apply for  $n > 1$ , and  $S_n$  saturates for  $t \rightarrow \infty$ , as discussed in section 3.2. The saturation values predicted by (19) are reported as horizontal dashed lines in Fig. 2. The deviations from (19) have to be interpreted

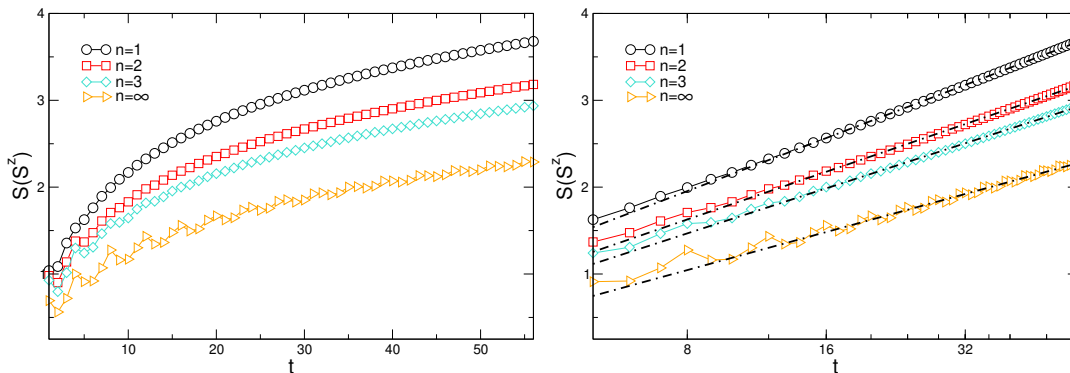


**Figure 3.** Dynamics of the Rényi operator entanglement entropies  $S_n$  for  $S^z$  in the rule 54 chain. Left panel:  $tDMRG$  data for  $S_n$  plotted versus time  $t$  and  $n = 1, 2, 3, \infty$ . Right panel: Same as in the left panel using the logarithmic scale on the  $x$ -axis. The dash-dotted lines are fits to  $S_n = a \ln(t) + b$ , with  $a, b$  fitting parameters.

as finite-time corrections. Corrections are more precisely investigated in the right panel of Fig. 2 plotting  $S_n - n/(n-1) \ln(2)$  versus  $1/t$ . A fit of the data at long times to the behavior  $\sim t^{-\alpha}$  gives  $\alpha \approx 1/2$ . This motivates the ansatz for  $S_n$  as

$$S_n = \frac{n}{n-1} \ln(2) + \frac{a_1}{t^{1/2}} + \frac{a_2}{t}, \quad (23)$$

with  $a_1, a_2$  fitting parameters. As it is clear from Fig. 2, the fits are in satisfactory agreement with the numerical data, confirming that  $S_n$  saturate to a constant in the limit  $t \rightarrow \infty$ . We anticipate that the saturating behavior of  $S_n$  for  $n > 1$  is also confirmed by the behavior of the operator entanglement spectrum (see Section 4.3).

#### 4.2. Non CFT scaling of the OSE of traceless operators?

Having discussed the Rényi entropies of  $P_z$ , we now focus on its traceless part  $S^z$ . In Fig. 3 we show  $tDMRG$  data for the rule 54 chain. Our data are obtained by employing bond dimension  $\chi = 1600$ . In contrast with the projector operator  $P_z$  (see Fig. 2), now  $S_n$  grow logarithmically also for  $n > 1$ . This is confirmed in the right panel of Fig. 3 plotting  $S_n$  versus time by using a logarithmic scale on the  $x$ -axis. The dashed-dotted lines in Fig. 3 are fits to the behavior (22). We now obtain  $a = 0.92(2), 0.80(5), 0.76(5), 0.64(5)$  for  $n = 1, 2, 3, \infty$ . Notice that for  $n = 1$  the fit gives  $a = 0.92(2)$ , which appears to be different from  $a = 1$ . This is also in contrast with what one should expect from (18), which would give  $a \approx 1$  since for  $P_z$  one has  $a \approx 0.5$ . Still, the discrepancy could be attributed to the systematic error due to finite-time corrections.

Let us consider the scaling of the moments  $M_n$  of the  $\lambda_i$  (cf. (2)), which form the operator entanglement spectrum.  $M_n$  are defined as

$$M_n := \sum_i \lambda_i^n. \quad (24)$$

Clearly,  $M_n$  contain the same information about the distribution of the ES levels as the Rényi entropies. The moments  $M_n$  for the operator  $S_z$  are plotted in Fig. 4. In

the Figure we show  $M_n$  versus time for several values of  $n$ , employing a logarithmic scale on both axis. First, the data exhibit a clear power-law behavior with increasing  $t$ . Moreover, for  $n < 1$ ,  $M_n$  increases with time, whereas for  $n > 1$ ,  $M_n$  vanishes in the limit  $t \rightarrow \infty$ . The exponent of the power-law depends on  $n$ , reflecting that the prefactor of the logarithmic growth of  $S_n$  depends on  $n$  (see Fig. 8). For  $n = 1$ , one has the normalization  $M_1 = 1$  (not shown in the Figure). In the limit  $n \rightarrow \infty$  a fit to the power-law behavior suggests the decay as  $t^{-2/3n}$ . The large  $n$  limit is confirmed in the inset of Fig. 4, where we plot  $\lambda_1$  versus  $t$ . The dotted and the dashed-dotted lines are the behaviors as  $t^{-1/2}$  and  $t^{-2/3}$ , respectively.

Let us assume that  $M_n$  for large  $t$  have the power-law behavior as

$$M_n \sim t^{-f_n}. \quad (25)$$

It is natural to conjecture that  $f_n$  is of the form

$$f_n = na_0 + \frac{a_1}{n} + \frac{a_2}{n^2} + \dots, \quad (26)$$

where the dots are for higher powers of  $1/n$ . Eq. (26) is reminiscent of the *CFT* scaling of the moments of the ground-state ES spectrum [39]. Precisely, in *CFT*s one has that only  $a_0$  and  $a_1$  are nonzero, and  $a_1 = -a_0$ , with  $a_0$  related to the central charge of the *CFT*. Let us now consider the limit  $n \rightarrow 1$  to recover the von Neumann *OSE*. If we assume that only  $a_0, a_1$  are nonzero in (26), one has  $S_1 \sim 2a_0 \ln(t)$ . Fig. 3 suggests the behavior  $S_1 \sim \ln(t)$ , whereas from Fig. 4 we have  $\lambda_1 \sim t^{-2/3}$ , implying  $a_0 > 1/2$ . This discrepancy could signal that the terms  $a_j$  with  $j > 1$  in the expansion (26) are nonzero. Finally, we should stress that *CFT*-like scaling was demonstrated for the growth of Rényi entropies of string operators in the *XX* chain [13].

### 4.3. Operator entanglement spectrum (ES)

Let us now consider the operator entanglement spectrum (*ES*). The levels  $\xi_i$  of the *ES* are defined as

$$\xi_i = -\ln(\lambda_i), \quad (27)$$

with  $\lambda_i$  the squared singular values in (2). In Fig. 5 we focus on the dynamics of the entanglement spectrum of  $P_z$  and of  $S^z$  (left and right panels, respectively). Notice that  $P_z$  and  $S^z$  differ by  $1/2\mathbb{1}$ , and the results of Section 3.2 should hold. The *ES* levels exhibit a nontrivial dynamics. Upon increasing time, there are more and more levels that contribute to the *ES*. Let us focus on the operator entanglement spectrum of  $P_z$  (left panel in Fig. 5). The smallest *ES* level is  $-\ln(\lambda_1) \approx \ln(2)$ , reflecting the behavior  $S_\infty \rightarrow \ln(2)$  for  $t \rightarrow \infty$ , which we observed in Fig. 3 (right panel). The *ES* levels above the lowest one are strongly suppressed. For instance, for  $t = 40$  they are  $-\ln(\lambda_2) \approx 2.7$ . This is in agreement with the decomposition (17).

Moreover, according to (17) one can obtain the operator *ES* of  $P_z$  from that of  $S^z$ . Indeed, one should expect that (cf. (17))

$$\lambda_i = \left\{ \frac{1}{2}, \frac{1}{2} \lambda_i' \right\}, \quad (28)$$

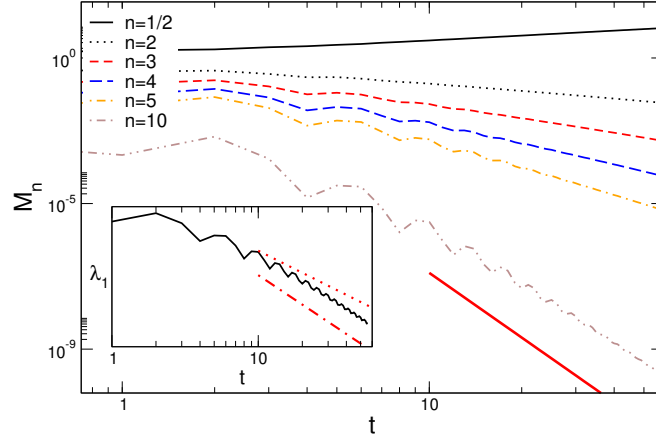


**Figure 4.** Moments  $M_n$  of the squared singular values  $\lambda_i$  (cf. (2)) for the dynamics of the operator  $S^z$  in the rule 54 chain. We plot  $M_n$  as functions of time  $t$  and for several values of  $n$ . Notice the logarithmic scale on both axes. The thick red line is the behavior  $t^{-2/3n}$  for  $n = 10$ . The inset shows the largest Schmidt value  $\lambda_1$  as a function of  $t$ . The dotted line and the dashed-dotted lines are the behaviors  $t^{-1/2}$  and  $t^{-2/3}$ , respectively.

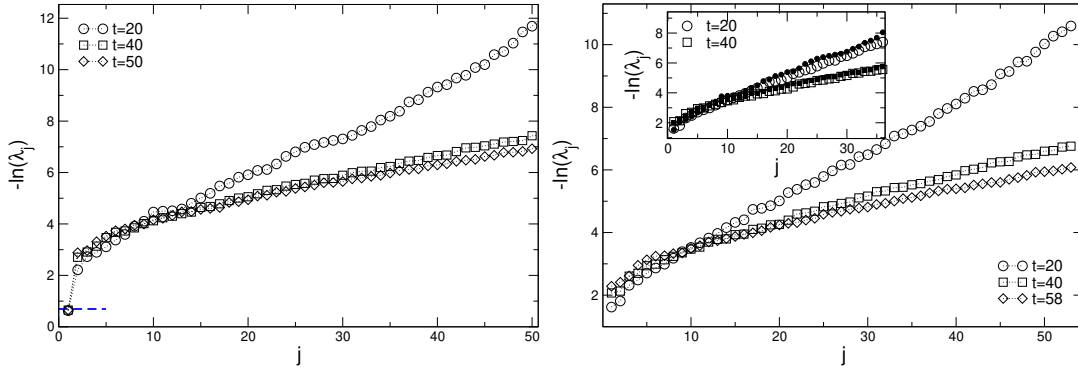


**Figure 5.** Dynamics of the operator entanglement spectrum in the rule 54 chain. Both panels show  $tDMRG$  results with bond dimension  $\chi = 1600$ . Left panel: Operator entanglement spectrum for the projector operator  $P_z$ . The  $y$ -axis shows  $-\ln(\lambda_j)$ , with  $\lambda_j$  the squared Schmidt values. On the  $x$ -axis  $j$  is a label for the entanglement spectrum levels. The different symbols are for different times. Right panel: Same as in the left panel for the operator  $S^z$ . Inset: Comparison between the  $ES$  levels  $-\ln(\lambda'_j)$  of  $S^z$  (empty symbols) and the shifted  $ES$  levels  $-\ln(\lambda_j) - \ln(2)$  of  $P_z$ .

with  $-\ln(\lambda'_i)$  forming the  $ES$  of  $S^z$  and  $\lambda_i$  that of  $P_z$ . The operator  $ES$  of  $S^z$  is reported in the right panel in Fig. 5. Now the  $ES$  level  $\lambda_1 = \ln(2)$  is not present, in contrast with the  $ES$  of  $P_z$  (left panel in the Figure). In the inset we show the  $ES$  levels for  $S^z$  for  $t = 20, 40$  (empty symbols). These are the same data reported in the main Figure. We also show the shifted levels  $-\ln(\lambda_i) - \ln(2)$  with  $\lambda_j$  forming the  $ES$  of  $P_z$ . Interestingly, they match the  $ES$  of  $S^z$  quite accurately, and the agreement improves at longer times.

Finally, it is interesting to discuss the distribution of  $ES$  levels. Since the  $ES$  of



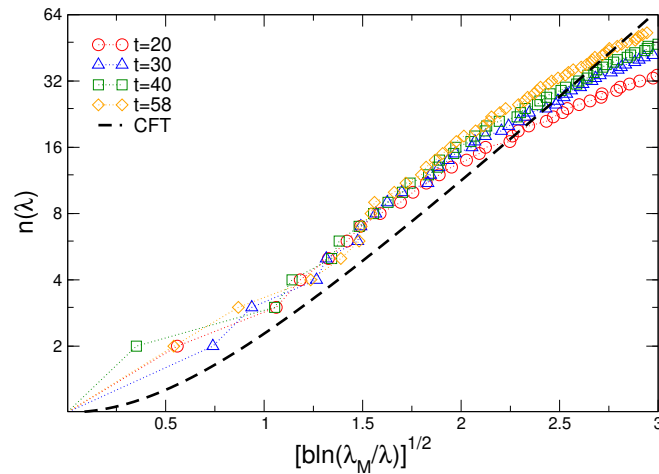


**Figure 6.** Dynamics of the operator entanglement spectrum levels in the rule 54 chain. We show  $tDMRG$  data at fixed bond dimension  $\chi = 1600$  for the operator  $S^z$ . We plot  $n(\lambda)$ , i.e., the number of  $ES$  levels smaller than  $\lambda$ , as a function of the scaling variable  $\xi = \sqrt{b \ln(\lambda_M/\lambda)}$ , with  $b := -\ln(\lambda_M)$ , and  $-\ln(\lambda_M)$  the lowest  $ES$  level. Different symbols correspond to different times. The dashed line is (29), i.e., the  $CFT$ -like scaling.

operators with nonzero trace can be derived from that of their traceless part, we focus on  $S^z$ . We consider the number of  $ES$  levels  $n(\lambda)$ , which are larger than  $\lambda$ . In critical ground states described by  $CFT$ s, it has been shown that [39]

$$n(\lambda) = I_0(2\xi), \quad \xi := \sqrt{b \ln(\lambda_M/\lambda)}, \quad (29)$$

where  $\lambda_M$  is the largest eigenvalue of the  $ES$ ,  $b = -\ln(\lambda_M)$ , and  $I_0$  is the modified Bessel function of the first kind. Eq. (29) implies that  $n(\lambda)$  is “superuniversal”, because it depends only on the central charge of the  $CFT$ , which is encoded in the scaling of  $\lambda_M$ .

In Fig. 6 we plot  $n(\lambda)$  as a function of  $\xi$ . The different symbols correspond to different times. At long times the data exhibit scaling collapse. This could suggest that although the moments  $M_n$  do not scale as in  $CFT$  (see Fig. 6),  $n(\lambda)$  is a function of  $\xi$ , at least in the limit  $t \rightarrow \infty$ . The dashed line in Fig. 6 is the prediction in  $CFT$  systems  $n(\lambda) = I_0(2\xi)$  (cf. (29)). Fig. 6 shows strong deviations from (29). This reflects that the moments  $M_n$  (cf. (25)) do not obey  $CFT$  scaling, which is given by Eq. (26) with  $a_j = 0$  for  $j > 1$  and  $a_1 = -a_0$ .

## 5. Rényi OSE entropies in the deformed $XXZ$ chain: $tDMRG$ results

We now focus on the operator spreading in the deformed  $XXZ$  chain (cf. (9)). We first consider the integrable case with  $\Delta' = 0$ , i.e., the  $XXZ$  chain. In section 5.1 we show that the decomposition (17) holds true also for the  $XXZ$  chain, similar to the rule 54 chain (see section 4.1). In section 5.2 we investigate the effect of  $\Delta'$ , which breaks

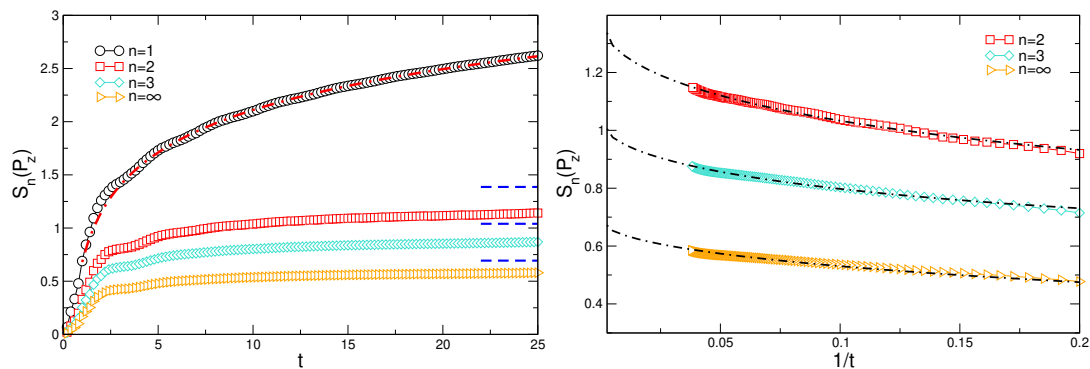


**Figure 7.** Dynamics of the Rényi operator entanglement entropies  $S_n$  for the projector operator  $P_z$  in the  $XXZ$  spin chain with  $\Delta = 10$ . Left panel:  $tDMRG$  data for  $S_n$  plotted versus time  $t$ . The dashed-dotted line is a fit to  $S_1 = a \ln(t) + b$ , with  $a, b$  fitting parameters. For  $n = 1$  the fit gives  $a \approx 1/2$ . The dashed lines are (19). Right panel: Same as in the left panel using the logarithmic scale on the  $x$ -axis. The dashed-dotted lines are fits to  $S_n = n/(n-1) \ln(2) + a_1/t^{1/2} + a_2/t$ , with  $a_1, a_2$  fitting parameters.

the integrability. Finally, in section 5.3 we investigate revivals in the  $OSE$  entropies in finite-size systems, showing that they can distinguish integrable from non-integrable dynamics.

### 5.1. Traceless versus operators with nonzero trace

Let us consider the Rényi entropies  $S_n$  of the projector operator  $P_z$  in the  $XXZ$  chain. We report  $tDMRG$  data in Fig. 7 plotting  $S_n(P_z)$  versus time for  $n = 1, 2, 3, \infty$ . The data are for the  $XXZ$  chain with  $\Delta = 10$ . Clearly,  $S_1(P_z)$  increases logarithmically with time (see left panel in Fig. 7). The dashed-dotted line in the figure is a fit to the behavior  $S_1 = a \ln(t) + b$ , with  $a, b$  fitting parameters. The fit gives  $a \approx 1/2$  in agreement with the results of Ref. [15]. For  $n > 1$ , the dynamics of  $S_n$  is compatible with a saturation at  $t \rightarrow \infty$ , similar to the rule 54 chain (see Section 4). In the right panel of Fig. 7 we plot  $S_n - n/(n-1) \ln(2)$  versus  $1/t$  for  $n = 2, 3, \infty$ . The dashed dotted lines are fits to

$$S_n = \frac{n}{n-1} \ln(2) + \frac{a_1}{t^{1/2}} + \frac{a_2}{t}, \quad (30)$$

with  $a_1, a_2$  fitting parameters. The behavior of the corrections as  $1/t^{1/2}$  is motivated by the results for the rule 54 chain (see Fig. 2). The dashed-dotted lines are obtained by fitting the data in the interval  $1/t \in (0, .1]$ . The agreement with (30) is satisfactory, confirming that the data are compatible with  $S_n(t) \rightarrow n(n-1) \ln(2)$  for  $t \rightarrow \infty$ .

Let us now consider the operator  $S^z$ . In Fig. 8 we show  $tDMRG$  data for  $S_n$  for the  $XXZ$  chain with  $\Delta = 10$ . In contrast with the case of  $P_z$  the left panel of Fig. 8 suggests that  $S_n$  grows with time for any  $n$ , as for the rule 54 chain. This is supported in the right panel of Fig. 8 plotting  $S_n$  versus  $t$  and using a logarithmic scale on the  $x$  axis. The dashed-dotted lines in Fig. 9 are fits to

$$S_n = a \ln(t) + b + \frac{c}{t^{1/2}}, \quad (31)$$

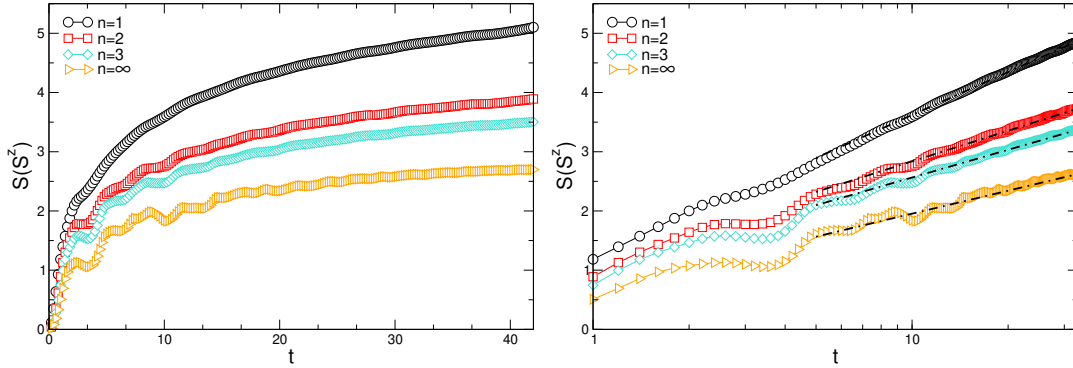


**Figure 8.** Dynamics of the Rényi operator entanglement entropies  $S_n$  for the projector operator  $S_z$  in the  $XXZ$  spin chain with  $\Delta = 10$ . Left panel:  $t$ DMRG data for  $S_n$  plotted versus time  $t$ . Right panel: Same as in the left panel using the logarithmic scale on the  $x$ -axis. The dash-dotted lines are fits to (31).

with  $a, b, c$  fitting parameters. By fitting the data with  $t > 10$  we obtain  $a = 1.05(5), 0.70(5), 0.66(5), 0.50(5)$  for  $n = 1, 2, 3, \infty$ . Interestingly, the fitted values of  $a$  are consistent with the results obtained for the rule 54 chain (see Section 4), although the time scales that are accessible are not enough to clarify whether they are the same.

It is interesting to discuss the validity of the bound in Eq. (10), and whether it is saturated. Given an operator  $\hat{O}$  with  $OTOC$  as  $\langle \hat{O}(t)\hat{O}(0) \rangle \sim t^{-\alpha}$ , with  $\alpha > 0$ , if we assume that the bound (10) is saturated we obtain

$$S_n \sim \frac{2\alpha n}{n-1} \ln(t). \quad (32)$$

For  $\alpha = 1$  and  $\alpha = 1/2$ , which correspond to ballistic and diffusive operator spreading, Eq. (32) gives  $S_n \sim 2n/(n-1) \ln(t)$  and  $S_n \sim n/(n-1) \ln(t)$ , respectively. Now, for  $n = 2$ , Eq. (32) implies that  $S_2 \sim 4 \ln(t)$  and  $S_2 \sim 2 \ln(t)$  for  $\alpha = 1$  and  $\alpha = 1/2$ , respectively. On the other hand, from Fig. 8 one obtains the milder increase as  $S_2 \sim 0.8 \ln(t)$ . This confirms that the bound (10) is not saturated, at least for integrable systems.

## 5.2. Breaking integrability

For generic nonintegrable systems, according to the membrane picture for entanglement spreading,  $S_1$  grows linearly with time [26]. The key assumption of the membrane picture is that the entanglement profile  $S_1(x, t)$ , with  $x$  denoting the position of the cut dividing subsystem  $A$  and  $B$  (see Fig. 1), satisfies an equation of the form  $\partial_t S_1(x, t) = s_{\text{eq}} \Gamma(\partial_x S_1(x, t))$ , with  $\Gamma$  the entropy production rate, and  $s_{\text{eq}}$  the density of entanglement entropy at equilibrium [25]. Under quite general assumptions on  $\Gamma$ , the membrane picture predicts linear growth of the entropy. On the other hand, as it was stressed in Section 3.1, even in nonintegrable systems it is possible to derive a logarithmic bound for the growth of the Rényi OSE entropies for operators that are linked with a conserved quantity [38] and exhibit a power-law decaying  $OTOC$ . To investigate

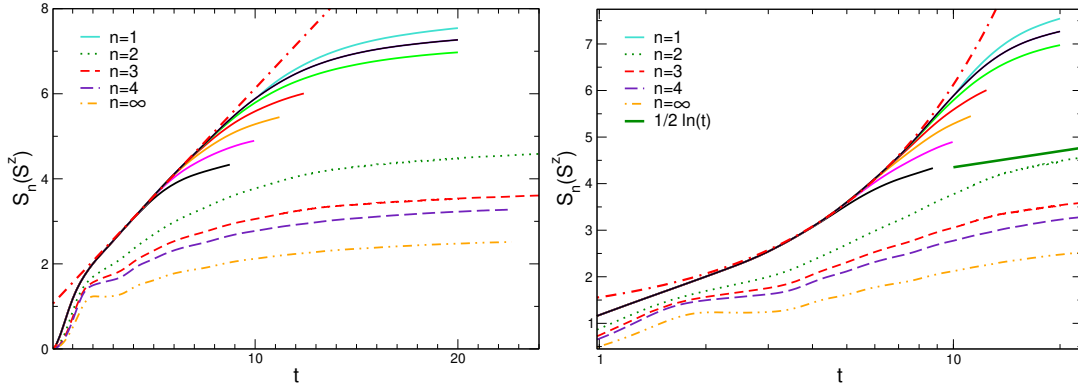


**Figure 9.** Dynamics of the Rényi operator entanglement entropies  $S_n$  for  $S^z$  in the nonintegrable  $XXZ$  chain with  $\Delta = 3$  and  $\Delta' = 0.25\Delta$  (cf. (9)). Left panel:  $tDMRG$  data for  $S_n$  as a function of time  $t$ . For  $n = 1$  (continuous lines) the different curves correspond to different bond dimensions  $\chi = 50, 100, 200, 400, 800, 1600, 2500$  (from bottom to top). The dash-dotted line is to highlight linear behavior at short times. The remaining curves are  $S_n$  with  $n = 2, 3, 4, \infty$ . For  $n > 1$  we show data for  $\chi = 1600$ . Right panel: Same data as in the left panel using the logarithmic scale on the  $x$ -axis.

operators spreading in the presence of integrability-breaking perturbations, in Fig. 9 we plot  $S_n(S^z)$  for the deformed  $XXZ$  chain (cf. (9)) with  $\Delta = 3$  and  $\Delta' = 1/4\Delta$ . For nonzero  $\Delta'$  the Hamiltonian in Eq. (9) is nonintegrable. In particular, by using standard diagnostic tools for chaotic systems, such as the distribution of energy levels, one can check that the spectrum of (9) is compatible with that of a chaotic Hamiltonian. In Fig. 9 we show the von Neumann entropy for several values of the bond dimension  $\chi = 50, 100, 200, 400, 800, 1600, 2500$  (continuous lines from bottom to top). As already discussed in Ref. [15], it is challenging to obtain the asymptotic behavior of  $S_1$  at  $t \rightarrow \infty$ . Precisely, the data at  $t \lesssim 10$  suggest a linear increase (see dashed-dotted line in the Figure). However, it is not clear whether the bending of the curves at long times signals a change in the behavior of  $S_1$ , or it is due to truncation of the bond dimension. In Fig. 9 we also show results for  $S_n$  with  $n = 2, 3, 4, \infty$ . Now, the growth of  $S_n$  is much weaker. We observe that the convergence with increasing  $\chi$  is faster. This is expected because the Rényi entropies are more sensitive to the lower part of the  $ES$ , which is better captured even at small  $\chi$ . Indeed, in Fig. 9 the data for  $S_n$  with  $n > 2$  are obtained with  $\chi = 1600$ . Now, in contrast with  $S_1$ ,  $S_n$  are compatible with a logarithmic increase for  $n > 1$ . Indeed, since the global magnetization is preserved by (9), even for nonzero  $\Delta'$ , it is reasonable to expect a power-law decaying  $OTOC$ . In turn, this implies (cf. (10)) at most logarithmic growth of the  $OSE$  entropies of  $S^z$ . This is also confirmed in the right panel of Fig. 9 where we employ a logarithmic scale on the  $x$  axis. Notice that the prefactor of the putative logarithmic growth is  $\sim 1/2 \ln(t)$ , i.e., even smaller than in the integrable case (see Fig. 8). Indeed, based on the behavior in Fig. 9, one cannot exclude that  $S_n$  saturate at long times.

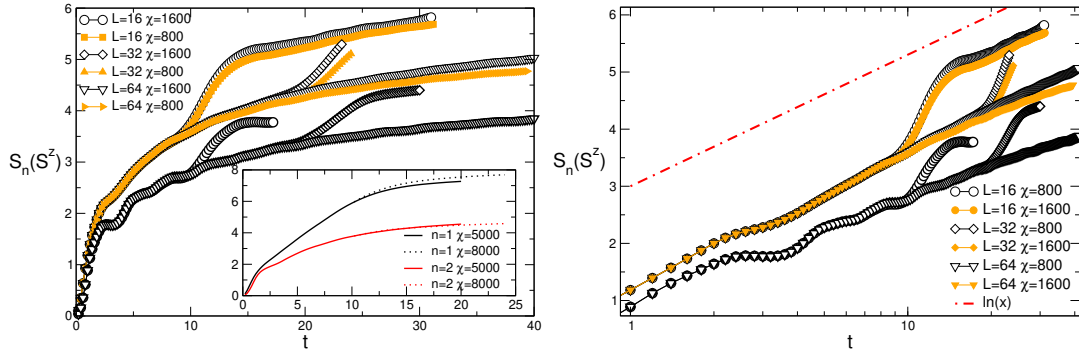


**Figure 10.** Revival effects in the dynamics of the operator entanglement  $S_n$  for  $S^z$ . Both panels show  $tDMRG$  data for the  $XXZ$  chain with  $\Delta = 3$ . Left panel: dynamics of  $S_n$  for a chain with  $L = 16, 32, 64$  (different symbols) and two values of the bond dimension  $\chi = 800, 1600$ . We show results for  $n = 1$  and  $n = 2$ . Revivals at  $t \approx L/2$  are visible. The inset shows the effect of integrability breaking. The curves are  $tDMRG$  data for the  $XXZ$  chain with  $\Delta = 3$  and  $\Delta' = 0.25\Delta$ . The data are for  $L = 16$  and  $n = 1, 2$  with  $\chi = 5000, 8000$ . The data show no revivals. Right panel: Same data as in the main left panel using the logarithmic scale on the  $x$ -axis. The dash-dotted line is  $\ln(t)$ .

### 5.3. Entanglement “revivals” & integrability breaking

It is interesting to investigate the effect of the finite-size of the chain in the dynamics of the operator entropies. It has been shown in Ref. [49] that in finite-size integrable chains the dynamics of the state entanglement after a global quantum quench exhibits “revivals”. The origin of revivals is that in integrable systems information spreads via the ballistic transport of quasiparticles. Moreover, quantum correlations between pairs of quasiparticles are preserved during their dynamics [1, 2, 5]. The entanglement between two spatial regions is due to entangled pairs that are shared between the regions. Now, if the regions are embedded in a *finite* chain the motion of the quasiparticles is periodic, implying periodicity in the contribution of the pairs to the entanglement between the regions. This explains revivals in the entanglement of a state. Notice that since not all the entangled pairs travel at the same velocity, the entanglement revivals weaken with the revival time [49]. This is a weak form of quantum information scrambling [50] for integrable systems. Oppositely, it was shown in Ref. [49] that for dynamics under nonintegrable Hamiltonians, revivals are more strongly suppressed. The reason is that entanglement dynamics in nonintegrable systems does not happen via quasiparticle spreading. Instead, information is quickly dispersed in the global degrees of freedom by the dynamics.

Here we show that revivals occur in the operator entanglement spreading in finite chains, although they have a different origin. In the following we focus on the dynamics of traceless operators in the deformed  $XXZ$  chain (9). Our  $tDMRG$  are reported in Fig. 10. In the left panel of Fig. 10 we plot  $S_n(S^z)$  for the  $XXZ$  chain with  $\Delta = 3$  ( $\Delta' = 0$  in (9)). We focus on  $n = 1$  and  $n = 2$ . We plot with different symbols (circles,

diamonds, and triangles) the dynamics in chains of different sizes  $L = 16, 32, 64$ . For  $n = 1$  the empty symbols correspond to  $\chi = 1600$ , whereas the full symbols are the results for  $\chi = 800$ . For  $n = 2$  we only show the results for  $\chi = 1600$ , because it is sufficient to ensure convergence. We plot the same data in the right panel in Fig. 10 using a logarithmic scale on the  $x$  axis. The revivals of the entropies are clearly visible. Interestingly, the prefactor of the logarithmic growth after the revival remains the same. Notice that the velocity of the quasiparticles, and hence the time of the revivals, could be determined via the Thermodynamic Bethe Ansatz approach [19]. Let us now discuss the mechanism underlying these revivals. First, as it is clear from the case of the rule 54 chain, (see Section 2.1), the growth of the entropies is not due to the propagation of entangled pairs. Instead, the growth of the *OSE* is due to the fact that the information needed to detect the position of the solitons generated by the operator insertion at the center grows with time. Now, the “kicks” at the revivals can be interpreted as the extra information needed to decide whether the solitons emitted at the center were reflected at the boundaries or not. Let us now discuss the effect of breaking integrability. We show *tDMRG* data for the nonintegrable *XXZ* chain with  $L = 16$  with  $\Delta = 3$  and  $\Delta' = \Delta/4$  in the inset of Fig. 10. The data do not show any sign of entanglement revivals. This is consistent with the fact that in nonintegrable systems information is not spread by propagation of quasiparticles.

## 6. Conclusions

We numerically investigated the dynamics of the Rényi Operator Space Entanglement (*OSE*) entropies in one dimensional systems. We focused on both integrable and nonintegrable systems. We first discussed the paradigmatic case of the rule 54 chain. We showed that the Rényi operator entanglement entropies  $S_n$  of traceless operators grow logarithmically with time for any  $n$ . The prefactor of the logarithmic growth depends on  $n$  in a nontrivial manner. On the other hand, for operators that have nonzero trace,  $S_n$  grow logarithmically only for  $n = 1$ . For  $n > 1$ ,  $S_n$  saturate in the limit  $t \rightarrow \infty$ , and the saturation values are determined by the operator trace. Moreover, our results suggest that the full entanglement spectrum of operators with nonzero trace can be reconstructed from the entanglement spectrum of their traceless part. Interestingly, the scenario is similar for the *XXZ* chain, which is a prototypical Bethe ansatz integrable model. Specifically, the entropies of operators with nonzero trace grow logarithmically for  $n = 1$ , whereas they saturate for  $n > 1$ . For traceless operators,  $S_n$  grows logarithmically for any  $n$ . The prefactors of the logarithmic growth are compatible with the ones numerically obtained for the rule 54 chain.

We next discussed operator spreading in nonintegrable dynamics. As it was shown in Ref. [15], it is challenging to extract the asymptotic behavior of  $S_1$  at long times. On the other hand, the growth of  $S_n$  for  $n > 1$  is milder as compared with  $n = 1$ , and it is compatible with a logarithmic growth, at least for the models that we considered. Finally, we showed that in finite integrable systems,  $S_n$  exhibit revivals. After the



revivals  $S_n$  continue growing logarithmically with time. Interestingly, upon switching on integrability-breaking interactions, revivals disappear, signaling the absence of well-defined quasiparticles.

There are several directions for future research. First, it is important to clarify the scaling of the *OSE* entropies in nonintegrable systems. This is a challenging task, as already pointed out in Ref. [15], because of strong finite-time corrections. Furthermore, it would be important to clarify the mechanism underlying the growth of *OSE* in integrable systems. Precisely, the fact that the prefactor of the logarithmic growth of the entropies is the same for both the rule 54 chain and the *XXZ* chain suggests that it could be universal. It would be useful to numerically extract the prefactor of the logarithmic growth by using the *MPO* representation of local operators [24, 14, 51] in the rule 54 chain. This will allow to clarify the relationship between *OSE* growth and transport properties. Notice that a deep relationship between operator growth and transport has been already established in Ref. [52] for some one-dimensional systems subject to dephasing. Finally, having access to the asymptotic behavior of the Rényi entropies would allow to reconstruct the structure of the operator entanglement spectrum.

## Acknowledgements

This study was carried out within the National Centre on HPC, Big Data and Quantum Computing - SPOKE 10 (Quantum Computing) and received funding from the European Union Next-GenerationEU - National Recovery and Resilience Plan (NRRP) – MISSION 4 COMPONENT 2, INVESTMENT N. 1.4 – CUP N. I53C22000690001. This work has been supported by the project “Artificially devised many-body quantum dynamics in low dimensions - ManyQLowD” funded by the MIUR Progetti di Ricerca di Rilevante Interesse Nazionale (PRIN) Bando 2022 - grant 2022R35ZBF.

## References

- [1] Calabrese P and Cardy J 2005 *Journal of Statistical Mechanics: Theory and Experiment* **2005** P04010 URL <https://doi.org/10.1088/1742-5468/2005/P04010>
- [2] Fagotti M and Calabrese P 2008 *Phys. Rev. A* **78**(1) 010306 URL <https://link.aps.org/doi/10.1103/PhysRevA.78.010306>
- [3] Kim H and Huse D A 2013 *Phys. Rev. Lett.* **111**(12) 127205 URL <https://link.aps.org/doi/10.1103/PhysRevLett.111.127205>
- [4] Liu H and Suh S J 2014 *Phys. Rev. Lett.* **112**(1) 011601 URL <https://link.aps.org/doi/10.1103/PhysRevLett.112.011601>
- [5] Alba V and Calabrese P 2017 *Proceedings of the National Academy of Sciences* **114** 7947–7951 ISSN 0027-8424 (*Preprint* <https://www.pnas.org/content/114/30/7947.full.pdf>) URL <https://www.pnas.org/content/114/30/7947>
- [6] Bertini B, Klobas K, Alba V, Lagnese G and Calabrese P 2022 *Phys. Rev. X* **12**(3) 031016 URL <https://link.aps.org/doi/10.1103/PhysRevX.12.031016>
- [7] Schollwöck U 2011 *Annals of Physics* **326** 96–192 ISSN 0003-4916 january 2011 Special Issue URL <https://www.sciencedirect.com/science/article/pii/S0003491610001752>



- [8] Paeckel S, Köhler T, Swoboda A, Manmana S R, Schollwöck U and Hubig C 2019 *Annals of Physics* **411** 167998 ISSN 0003-4916 URL <https://www.sciencedirect.com/science/article/pii/S0003491619302532>
- [9] Prosen T and Žnidarič M 2007 *Phys. Rev. E* **75**(1) 015202 URL <https://link.aps.org/doi/10.1103/PhysRevE.75.015202>
- [10] Zanardi P 2001 *Phys. Rev. A* **63**(4) 040304 URL <https://link.aps.org/doi/10.1103/PhysRevA.63.040304>
- [11] Prosen T and Pižorn I 2007 *Phys. Rev. A* **76**(3) 032316 URL <https://link.aps.org/doi/10.1103/PhysRevA.76.032316>
- [12] Pižorn I and Prosen T 2009 *Phys. Rev. B* **79**(18) 184416 URL <https://link.aps.org/doi/10.1103/PhysRevB.79.184416>
- [13] Dubail J 2017 *Journal of Physics A: Mathematical and Theoretical* **50** 234001 URL <https://dx.doi.org/10.1088/1751-8121/aa6f38>
- [14] Alba V, Dubail J and Medenjak M 2019 *Phys. Rev. Lett.* **122**(25) 250603 URL <https://link.aps.org/doi/10.1103/PhysRevLett.122.250603>
- [15] Alba V 2021 *Phys. Rev. B* **104**(9) 094410 URL <https://link.aps.org/doi/10.1103/PhysRevB.104.094410>
- [16] Bobenko Alexander and Bordemann M, Gunn C and Pinkall U 1993 *Communications in Mathematical Physics* **158** 127–134 ISSN 1432-0916 URL <https://doi.org/10.1007/BF02097234>
- [17] Buča B, Klobas K and Prosen T 2021 *Journal of Statistical Mechanics: Theory and Experiment* **2021** 074001 URL <https://dx.doi.org/10.1088/1742-5468/ac096b>
- [18] Gopalakrishnan S 2018 *Phys. Rev. B* **98**(6) 060302 URL <https://link.aps.org/doi/10.1103/PhysRevB.98.060302>
- [19] Gopalakrishnan S, Huse D A, Khemani V and Vasseur R 2018 *Phys. Rev. B* **98**(22) 220303 URL <https://link.aps.org/doi/10.1103/PhysRevB.98.220303>
- [20] Prosen T and Mejía-Monasterio C 2016 *Journal of Physics A: Mathematical and Theoretical* **49** 185003 URL <https://dx.doi.org/10.1088/1751-8113/49/18/185003>
- [21] Gopalakrishnan S and Zakirov B 2018 *Quantum Science and Technology* **3** 044004 URL <https://dx.doi.org/10.1088/2058-9565/aad759>
- [22] Buča B, Garrahan J P, Prosen T and Vanicat M 2019 *Phys. Rev. E* **100**(2) 020103 URL <https://link.aps.org/doi/10.1103/PhysRevE.100.020103>
- [23] Rowlands D A and Lamacraft A 2018 *Phys. Rev. B* **98**(19) 195125 URL <https://link.aps.org/doi/10.1103/PhysRevB.98.195125>
- [24] Klobas K, Medenjak M, Prosen T and Vanicat M 2019 *Communications in Mathematical Physics* **371** 651–688 ISSN 1432-0916 URL <https://doi.org/10.1007/s00220-019-03494-5>
- [25] Nahum A, Ruhman J, Vijay S and Haah J 2017 *Phys. Rev. X* **7**(3) 031016 URL <https://link.aps.org/doi/10.1103/PhysRevX.7.031016>
- [26] Jonay C, Huse D A and Nahum A 2018 Coarse-grained dynamics of operator and state entanglement (*Preprint* 1803.00089) URL <https://arxiv.org/abs/1803.00089>
- [27] Chan A, De Luca A and Chalker J T 2018 *Phys. Rev. X* **8**(4) 041019 URL <https://link.aps.org/doi/10.1103/PhysRevX.8.041019>
- [28] von Keyserlingk C W, Rakovszky T, Pollmann F and Sondhi S L 2018 *Phys. Rev. X* **8**(2) 021013 URL <https://link.aps.org/doi/10.1103/PhysRevX.8.021013>
- [29] Zhou T and Nahum A 2020 *Phys. Rev. X* **10**(3) 031066 URL <https://link.aps.org/doi/10.1103/PhysRevX.10.031066>
- [30] Bertini B and Piroli L 2020 *Phys. Rev. B* **102**(6) 064305 URL <https://link.aps.org/doi/10.1103/PhysRevB.102.064305>
- [31] Bertini B, Kos P and Prosen T 2020 *SciPost Phys.* **8** 067 URL <https://scipost.org/10.21468/SciPostPhys.8.4.067>
- [32] Bertini B, Kos P and Prosen T 2020 *SciPost Phys.* **8** 068 URL <https://scipost.org/10.21468/>

[SciPostPhys.8.4.068](#)

- [33] Claeyns P W and Lamacraft A 2020 *Phys. Rev. Res.* **2**(3) 033032 URL <https://link.aps.org/doi/10.1103/PhysRevResearch.2.033032>
- [34] Foligno A, Zhou T and Bertini B 2023 *Phys. Rev. X* **13**(4) 041008 URL <https://link.aps.org/doi/10.1103/PhysRevX.13.041008>
- [35] Rampp M A, Moessner R and Claeyns P W 2023 *Phys. Rev. Lett.* **130**(13) 130402 URL <https://link.aps.org/doi/10.1103/PhysRevLett.130.130402>
- [36] Rampp M A, Rather S A and Claeyns P W 2024 *Phys. Rev. Res.* **6**(3) 033271 URL <https://link.aps.org/doi/10.1103/PhysRevResearch.6.033271>
- [37] Lopez-Piqueres J, Ware B, Gopalakrishnan S and Vasseur R 2021 *Phys. Rev. B* **104**(10) 104307 URL <https://link.aps.org/doi/10.1103/PhysRevB.104.104307>
- [38] Muth D, Unanyan R G and Fleischhauer M 2011 *Phys. Rev. Lett.* **106**(7) 077202 URL <https://link.aps.org/doi/10.1103/PhysRevLett.106.077202>
- [39] Calabrese P and Lefevre A 2008 *Phys. Rev. A* **78**(3) 032329 URL <https://link.aps.org/doi/10.1103/PhysRevA.78.032329>
- [40] Wigner E P 1955 *Phys. Rev.* **98**(1) 145–147 URL <https://link.aps.org/doi/10.1103/PhysRev.98.145>
- [41] Takahashi M 1999 *Thermodynamics of One-Dimensional Solvable Models* (Cambridge University Press)
- [42] Alba V and Calabrese P 2018 *SciPost Phys.* **4**(3) 17 URL <https://scipost.org/10.21468/SciPostPhys.4.3.017>
- [43] Bertini B, Collura M, De Nardis J and Fagotti M 2016 *Phys. Rev. Lett.* **117**(20) 207201 URL <https://link.aps.org/doi/10.1103/PhysRevLett.117.207201>
- [44] Castro-Alvaredo O A, Doyon B and Yoshimura T 2016 *Phys. Rev. X* **6**(4) 041065 URL <https://link.aps.org/doi/10.1103/PhysRevX.6.041065>
- [45] Mirsky L 1975 *Monatshefte für Mathematik* **79** 303–306 ISSN 1436-5081 URL <https://doi.org/10.1007/BF01647331>
- [46] Doyon B 2020 *SciPost Phys. Lect. Notes* **18** URL <https://scipost.org/10.21468/SciPostPhysLectNotes.18>
- [47] Vecchio G D V D and Doyon B 2022 *Journal of Statistical Mechanics: Theory and Experiment* **2022** 053102 URL <https://dx.doi.org/10.1088/1742-5468/ac6667>
- [48] Medenjak M 2022 *Journal of Physics A: Mathematical and Theoretical* **55** 404002 URL <https://dx.doi.org/10.1088/1751-8121/ac8fc4>
- [49] Modak R, Alba V and Calabrese P 2020 *Journal of Statistical Mechanics: Theory and Experiment* **2020** 083110 URL <https://dx.doi.org/10.1088/1742-5468/aba9d9>
- [50] Alba V and Calabrese P 2019 *EPL (Europhysics Letters)* **126** 60001 URL <https://doi.org/10.1209/0295-5075/126/60001>
- [51] Foligno A and Bertini B 2024 (*Preprint* **2408.16750**) URL <https://arxiv.org/abs/2408.16750>
- [52] Wellnitz D, Preisser G, Alba V, Dubail J and Schachenmayer J 2022 *Phys. Rev. Lett.* **129**(17) 170401 URL <https://link.aps.org/doi/10.1103/PhysRevLett.129.170401>